Transonic Unsteady Pressure Measurements on a Supercritical Airfoil at High Reynolds Numbers

Robert W. Hess,* David A. Seidel,† William B. Igoe,‡ and Pierce L. Lawing§
NASA Langley Research Center, Hampton, Virginia

Steady and unsteady pressures were measured on a two-dimensional supercritical airfoil in the NASA Langley Research Center 0.3 m Transonic Cryogenic Tunnel at Reynolds numbers of 6 to 35×10^6. The airfoil was oscillated in pitch at amplitudes of ±0.25 to ±1.0 deg at frequencies of 5–60 Hz. The special requirements of testing an unsteady pressure model in a pressurized cryogenic tunnel are discussed. Selected steady measured data are presented and are compared with GRUMFOIL calculations at Reynolds numbers of 6 and 30×10^6. Experimental unsteady results at Reynolds numbers of 6 and 30×10^6 are examined for Reynolds number effects. Measured unsteady results at two mean angles of attack at a Reynolds number of 30×10^6 are also examined.

Nomenclature

C_p = pressure coefficient
$|C_p|$ = modulus of oscillating pressure coefficient
C_l = lift coefficient
c = chord, in.
f = frequency, Hz
k = reduced frequency, based on semichord, $\pi cf/V$
M = Mach number
R = Reynolds number based on chord
V = velocity, in./s
x = streamwise coordinate measured from leading edge, in.
α = peak oscillation amplitude in pitch, positive leading edge up, deg
$\bar{\alpha}$ = steady or mean angle of attack, positive leading edge up, deg
ϕ = phase angle between oscillating pressure and oscillating wing angle of attack, deg

Subscripts

c = corrected value
t = test measurement

Introduction

THE advent of cryogenic wind tunnels has provided the capability to simulate flight equivalent conditions with reasonably sized models at relatively low dynamic pressures. In addition, the development of advanced miniature pressure transducers had enabled the measurement of unsteady pressures in a cryogenic environment. Utilizing these test advancements, a study was conducted in the 0.3 m Transonic Cryogenic Tunnel (0.3 m TCT) at the NASA Langley Research Center[1] to measure the unsteady pressure characteristics of a supercritical airfoil. This tunnel was used in the Advanced Technology Airfoil Test (ATAT) program in extensive steady flow airfoil studies that demonstrated the necessity for testing at high Reynolds numbers.[2] The airfoil used in the present unsteady tests is a 14% thick, supercritical airfoil, designated SC(2)-0714, which was developed at the NASA Langley Research Center.[3] As part of the ATAT program, this airfoil had previously been tested in the 0.3 m TCT to obtain steady flow characteristics.[4] The purpose of this test was to obtain unsteady transonic pressure measurements from an oscillating supercritical airfoil over a wide range of Reynolds numbers to supplement the previous steady flow results. A secondary objective of the test was the development of instrumentation techniques for measuring unsteady pressures at cryogenic temperatures.

The two-dimensional model had a 6 in. chord and an 8 in. span. The test was concentrated at a tunnel freestream Mach number of 0.72, which previous tests indicated to be the drag-rise Mach number. Reynolds number (based on a 6 in. chord) was varied from 6 to 35×10^6 and Mach number was varied at two Reynolds numbers. The range of test frequencies was 5–60 Hz at oscillating pitch amplitudes of ±0.25 to ±1.0 deg. In this paper, selected steady measured data are presented and are compared with GRUMFOIL calculations at Reynolds numbers of 6 and 30×10^6. Experimental unsteady results at Reynolds numbers of 6 and 30×10^6 are examined for Reynolds number effects. Measured unsteady results at two mean angles of attack at a Reynolds number of 30×10^6 are also discussed.

Apparatus

Model

The SC(2)-0714 model is shown in Fig. 1. It was machined from an alloy (Vascomax-200) that has superior dimensional stability properties at cryogenic conditions. A cavity machined

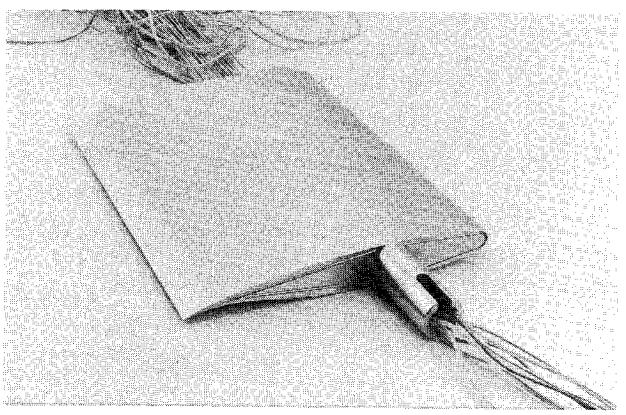

Fig. 1 External view of model.

Presented as Paper 87-0035 at the AIAA 25th Aerospace Sciences Meeting, Reno, NV, Jan. 12–15, 1987; received April 20, 1987; revision received Jan. 7, 1989.

*Senior Research Engineer (retired), Unsteady Aerodynamics Branch, Structural Dynamics Division. Member AIAA.
†Research Engineer, Unsteady Aerodynamics Branch, Structural Dynamics Division. Member AIAA.
‡Senior Research Engineer, Transonic Aerodynamics Division, High Reynolds Number Aerodynamics Branch. Member AIAA.
§Senior Research Engineer, Transonic Aerodynamics Division, High Reynolds Number Aerodynamics Branch. Senior Member AIAA.

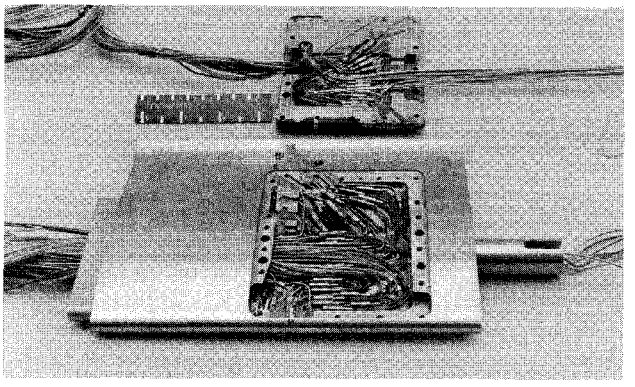

Fig. 2 Internal configuration of model.

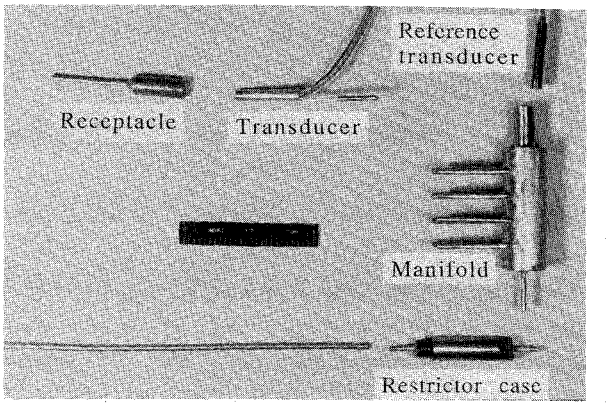

Fig. 4 Elements of the transducer system.

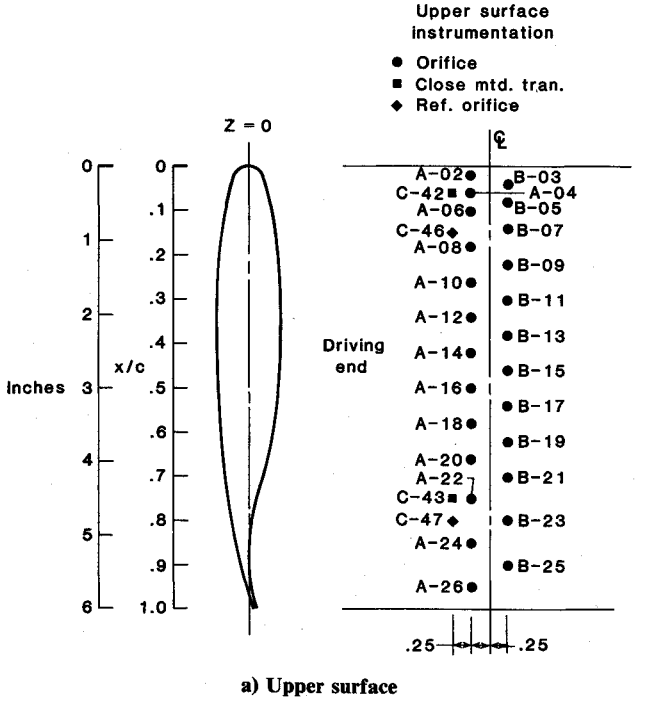

a) Upper surface

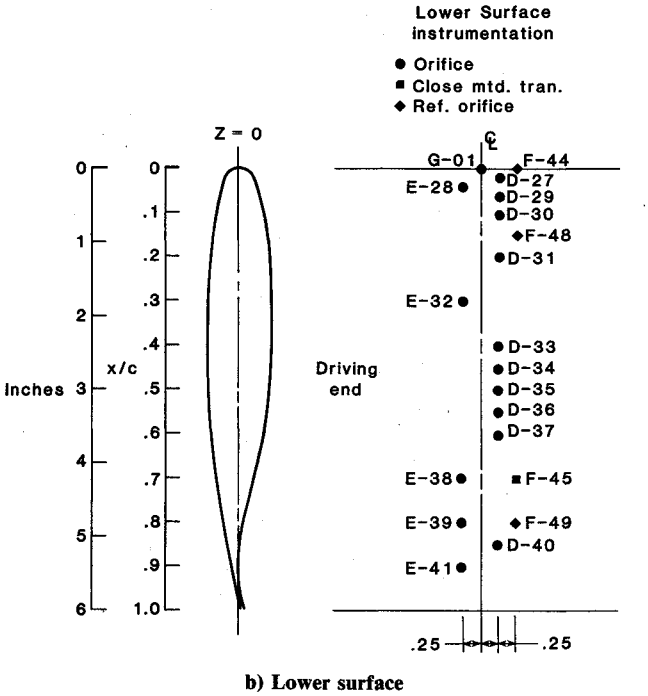

b) Lower surface

Fig. 3 Transducer locations.

in the underside of the wing (Fig. 2) provided the space necessary to mount the transducers. This cavity was closed by a cover plate on which some lower-surface transducers were mounted. The wing was supported on one end by a close-fitting tang fixed to a driving plate with machine screws; this end, seen on the left in Fig. 2, was sealed with epoxy. The other end was supported by an integral shaft that rotated in a bushing in the tunnel sidewall plate. A sliding seal of felt was used to seal the gap between the end of the oscillating airfoil and the fixed tunnel sidewall plate. The position of the supports was designed to locate the pitch axis at 35% chord.

Transducers

Forty-three unsteady pressure transducers were mounted internally in the model. Because of space constraints, 40 of the transducers were mounted in receptacles connected by a short length (nominally 0.75 in.) of tubing to the orifice. The remaining three transducers were mounted with the transducer head less than 0.1 in. below the surface of the wing. The orifices of these three transducers were paired with tube-mounted transducers for comparison purposes. A series of tests were conducted to examine the effects of orifice diameter, tube diameter, and tube length on the dynamic response of the system. At atmospheric conditions, there was no significant reduction of dynamic magnitude response or phase shift of the test configuration up to 100 Hz.

The location of the transducers is shown schematically in Fig. 3. The tube-mounted transducer orifices are located alternately in two rows 0.25 in. on either side of the centerline. On the top surface, the orifice distribution of the 25 transducers results in an orifice every 2% of chord to $x/c=0.1$, then 4% chord to $x/c=0.70$, and finally 5% chord to $x/c=0.95$. The distribution of the 15 tube-mounted transducer orifices on the lower surface is every 2% of chord to $x/c=0.06$ and is then 10% chord from $x/c=0.10$ to 0.90, with extra orifices located at $x/c=0.45$, 0.55, and 0.85. The close-mounted transducers and reference orifices are located 0.5 in. from the centerline.

The elements of the transducer system are shown in Fig. 4. Since the differential pressure between the wing surface and the tunnel static pressure could exceed the rated capability of the transducer, the transducer was referenced to one of five manifolds. In turn, each manifold was vented to one of the five reference orifices. A reference transducer was attached to each manifold to measure the pressure differential between the manifold and the tunnel static pressure.

The final configuration consisted of transducers with a 10 psi range and with outputs of between 5 and 9 mV/psi. Each transducer was mounted in a receptacle that, in turn, was connected to the 0.015 in. diam orifice by a 0.75 in. length of 0.030 in. i.d. tubing.

The connection between the manifold and the reference orifice was interrupted by a porous flow restrictor that damped out the oscillating pressure from the static reference orifice (replacing the long lengths of tubing usually used for

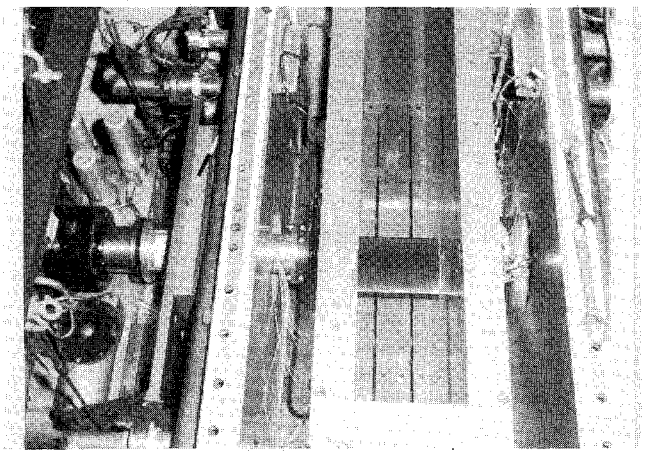

Fig. 5 Model installation.

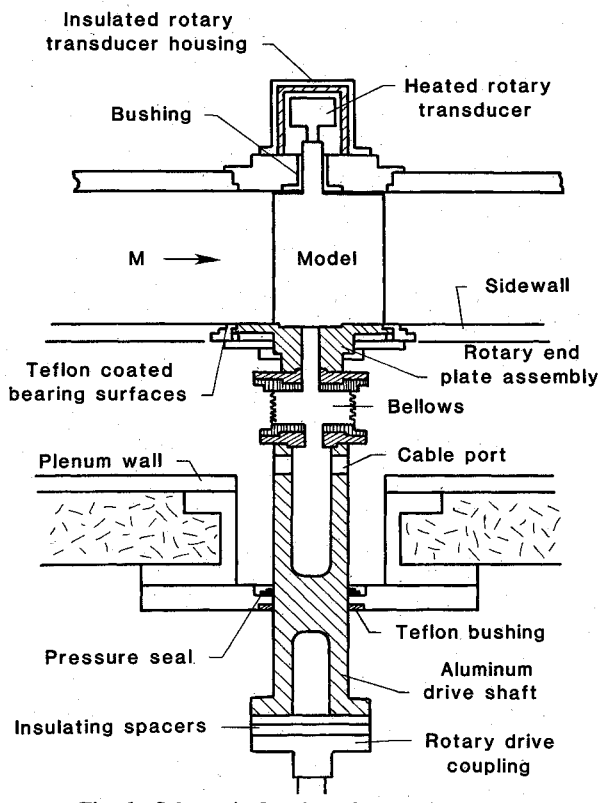

Fig. 6 Schematic drawing of model installation.

this purpose). Two 25 μm filters in series were selected for the wind-tunnel test. Because of lack of space in the model, the manifolds and flow restrictors were located outside the model during the test and were connected to the model with approximately 6 in. of tubing.

The transducers were to be recovered after the test and consequently could not be permanently bonded to the receptacle. A series of tests were conducted with candidate mastics and dummy transducers at 120 K and 20 psi pressure differential to determine which, if any, would maintain a seal after repeated cycling. A mastic supplied by the transducer vendor was selected for the installation.

Drive System

The large variations in temperature (120–320 K) and stagnation pressure (1.4–6 atm) over the operating range of the 0.3 m TCT result in sidewall deformations that required special considerations in the design of the oscillating drive system. Figure 5 shows the model and the drive system installation in the test section. The test section is shown to the right with the test section ceiling removed and can be identified by the two slots on

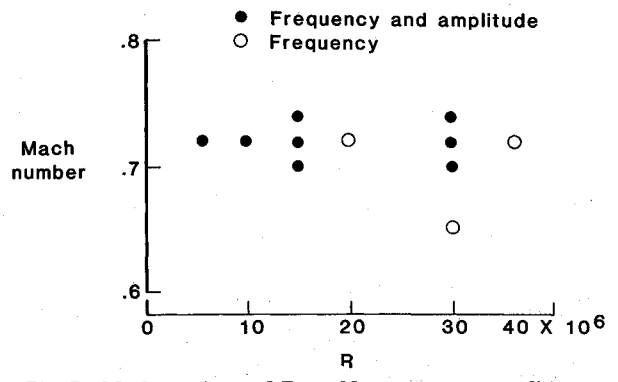

Fig. 7 Mach number and Reynolds number test conditions.

the floor that run under the model. The model is between the test section sidewalls, which in turn are between the tunnel plenum spaces and, finally, the tunnel pressure shell or plenum walls. The critical elements of the system are identified in the schematic drawing in Fig. 6. The hydraulic rotary actuator required the maintenance of precise alignment for the duration of the test. Since the 0.3 m TCT test section floats on a cable suspension system to accommodate thermal contraction at the cold operating conditions, the actuator and supporting structure were also supported by a system of cables, blocks, and counterweights so that they could move with the test section.

An insulating spacer between the actuator and the drive shaft and two hot-air blowers were used to reduce the chill on the actuator and system components external to the tunnel. A Teflon bushing and pressure seal were the remaining fixed support points for the hollow aluminum drive shaft. The shaft was attached to the rotating sidewall drive disk through a bellows that isolated the shaft from the relative in-line movement of the tunnel sidewall. The rotating drive disk was Teflon-coated on its circumferential bearing surfaces and had a rectangular slot to accommodate the wing tang. The tang was hollow to provide a path for transducer cables and tubing that went through a matching hole in the plate and exited through the cable ports in the drive shaft. This end of the wing was sealed with epoxy and bolted to the rotating disk.

The other end of the wing was supported by the integral hollow wing shaft and a bushing in the sidewall plate. This end of the wing moved relative to its mounting plate and was sealed with felt that matched the profile of the wing. The wing shaft was attached to a rotary transducer by an insulating shaft. The hollow wing shaft provided a path for the remaining instrumentation cables. The rotary transducer was heated with surface heaters under thermostat control and the entire assembly covered with an insulated can.

Data Acquisition and Reduction

Static data from the model and tunnel instrumentation were acquired using the 0.3 m TCT data acquisition system. The model angle of attack and pressure data were fed to the system's analog data acquisition channels. The system has 192 channels that are filtered with a 10 Hz low-pass filter and then digitized at 20 samples/s. Static data values are acquired by averaging the digitized values over a 1 s interval. The steady pressure data were integrated to obtain the normal-force coefficient, which is assumed equal to the lift coefficient.

Dynamic model data were acquired using analog tape recorders. The instrumentation signal was amplified to be a value of about 1 V rms. The model angle of attack and pressures were taken directly from the amplifiers and recorded on two 28 channel analog tapes operating at 15 in./s. To obtain magnitude and phase information at the frequency of oscillation and the lower harmonics, the data was digitized at 32 samples/cycle of oscillatory motion for 64 contiguous cycles. A fast Fourier transformation (FFT) was taken of the data to calculate the harmonic components of the unsteady pressures.

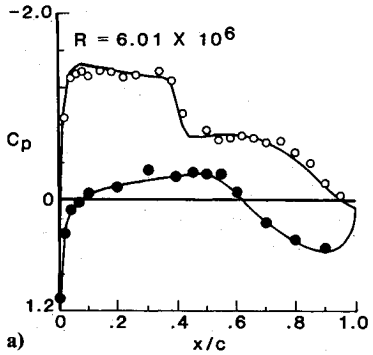

a)

	Tunnel	Corrected	Grumfoil
M	0.72	0.701	0.701
$\bar{\alpha}$	2.002	0.525	0.961
C_l	0.8523	0.8676	0.8757

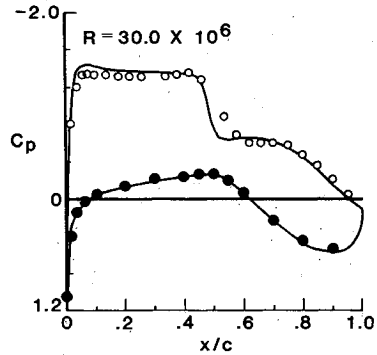

	Tunnel	Corrected	Grumfoil
M	0.721	0.705	0.705
$\bar{\alpha}$	1.997	0.393	0.910
C_l	0.926	0.939	0.9453

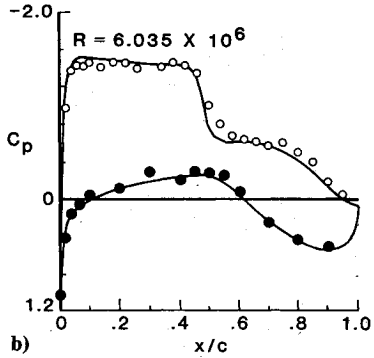

b)

	Tunnel	Corrected	Grumfoil
M	0.720	0.701	0.701
$\bar{\alpha}$	2.504	0.844	1.385
C_l	0.9581	0.9753	0.9837

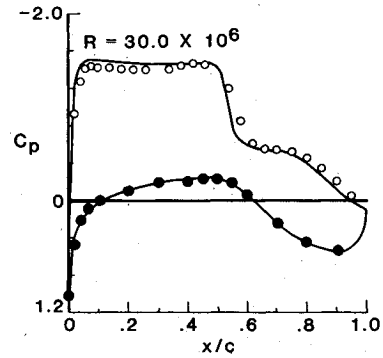

	Tunnel	Corrected	Grumfoil
M	0.719	0.705	0.705
$\bar{\alpha}$	2.51	0.756	1.399
C_l	1.0123	1.0256	1.0336

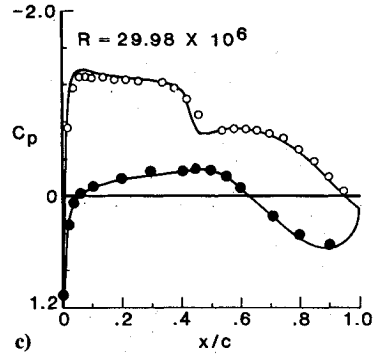

c)

	Tunnel	Corrected	Grumfoil
M	0.718	0.705	0.705
$\bar{\alpha}$	1.501	0.051	0.552
C_l	.8373	0.849	0.8555

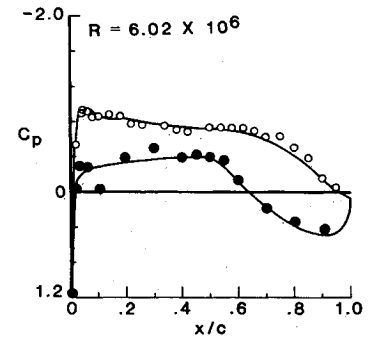

	Tunnel	Corrected	Grumfoil
M	0.720	0.701	0.701
$\bar{\alpha}$	0.004	-0.92	-0.398
C_l	0.5288	0.5383	0.5484

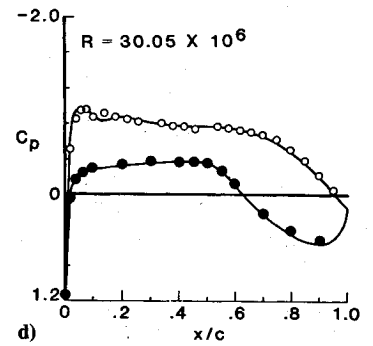

d)

	Tunnel	Corrected	Grumfoil
M	.721	0.705	0.705
$\bar{\alpha}$	-0.005	-1.036	-0.715
C_l	0.5951	0.6034	0.6099

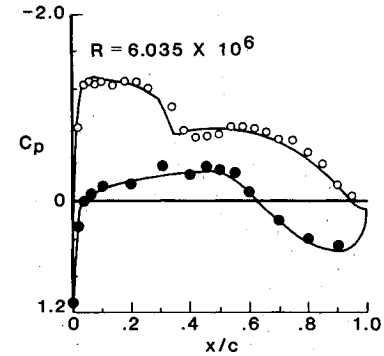

	Tunnel	Corrected	Grumfoil
M	0.719	0.701	0.701
$\bar{\alpha}$	1.495	0.201	0.493
C_l	0.7467	0.7601	0.7680

Fig. 8 Comparisons of steady test results (symbols) with calculated results (solid line) at a tunnel Mach number of 0.72, ◦ upper surface, • lower surface; a) $\bar{\alpha}_t \approx 2.5$ deg; b) $\bar{\alpha}_t \approx 2.0$ deg; c) $\bar{\alpha}_t \approx 1.5$ deg; d) $\bar{\alpha}_t \approx 0.0$ deg.

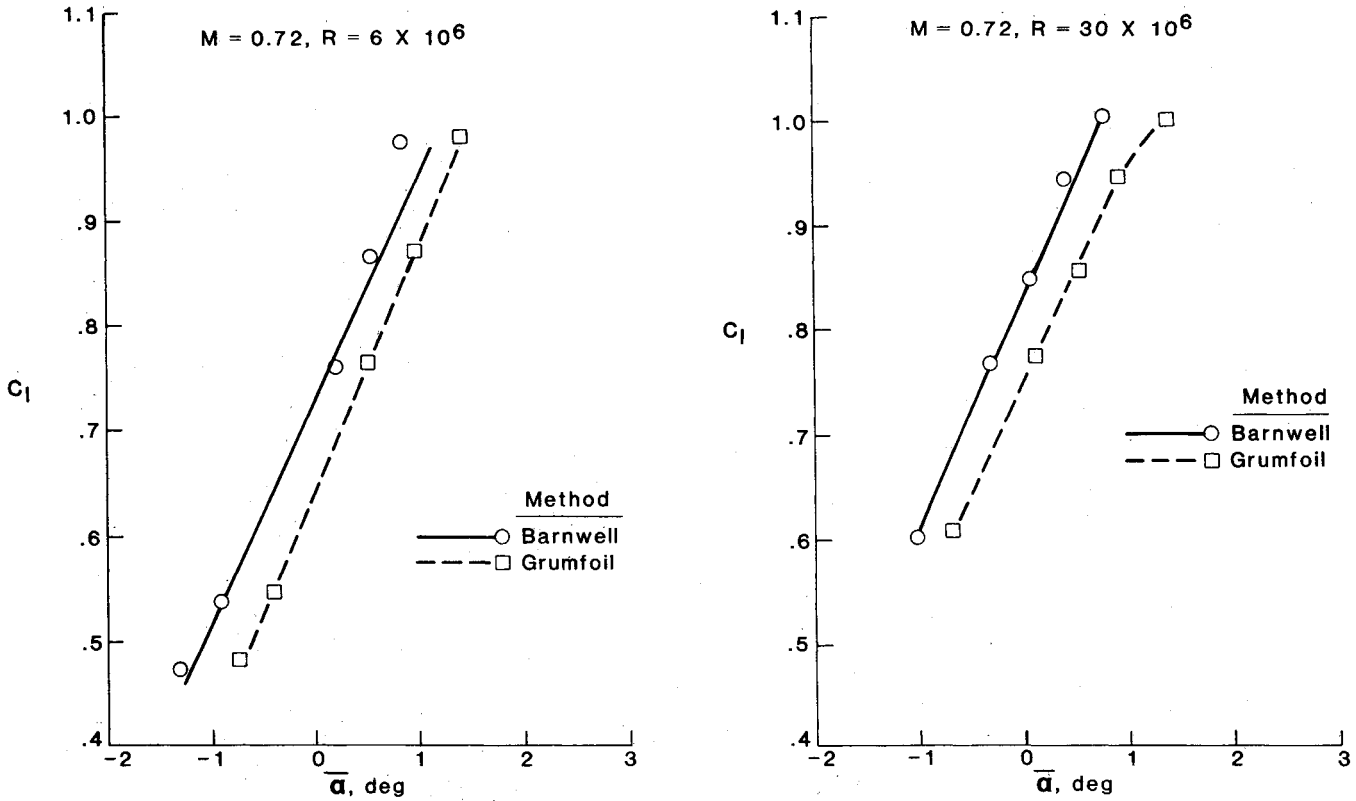

Fig. 9 Comparison of lift coefficient vs corrected angle of attack.

The data sample rate and number of cycles analyzed were selected to give an accurate estimate of the first three fundamental harmonic components. The harmonic pressure coefficients are normalized by the amplitude of the harmonic wing motion in degrees. All phase angles were relative to the wing position.

Sidewall boundary-layer and angle-of-attack corrections were applied to the measured steady pressure results. The sidewall boundary-layer corrections are based on the theory of Ref. 5, which is used in Ref. 6 with measured values of sidewall displacement and momentum thickness to compile the tables used to correct the experimental values in this paper. The angle-of-attack corrections described in Ref. 7 (sometimes referred to as the Barnwell-Davis-Moore correction) adjust the theory of Davis-Moore with experimental data. The wall-induced downwash immediately over the model for the 0.3 m TCT is

$$\Delta\bar{\alpha}=\frac{-C_l c}{8(1+j)h}$$

The parameters necessary to make the correction are $c=6$ in., $h=$ tunnel semiheight, 12 in., $a=$ slot spacing, 4 in., $\delta=$ width of slot $=0.2$ in., and $j=aK/h$, $K=3.2$ (semiempirical constant, function of δ and a). For $C_l=1.0$, $\Delta\bar{\alpha}=-1.73245$ deg.

Results and Discussion

The test was designed to explore the effects of Reynolds number on unsteady pressures and to generate a data base for validating unsteady aerodynamic computer codes. The boundary-layer transition was free during the test. The test conditions as defined by Mach number and Reynolds number are shown in Fig. 7. Test points were taken at the drag-rise Mach number of 0.72 at test Reynolds numbers varying from 6 to 35×10^6. Mach number was varied at two Reynolds numbers, 15 and 30×10^6. A total of 976 test points were taken. The primary data base was taken for pitch oscillation frequency between 5 and 40 Hz at an amplitude of ±0.25 deg, as indicated by the open and closed symbols. Once these data were in hand, the pitch amplitude was increased to ±0.5 and ±1.0 deg and the oscillation frequency to 60 Hz at test conditions indicated by the solid symbols.

Steady Pressures

Steady pressure distributions for four angles of attack $\bar{\alpha}_t$ of approximately 2.5, 2.0, 1.5, and 0 deg and for Reynolds numbers 6 and 30×10^6 are shown in Fig. 8. The experimental data are shown as symbols and the calculations as solid lines. The pressure data have been corrected for sidewall effects[5,6] and angle of attack.[7] Calculated pressure distributions from the full potential GRUMFOIL computer code[8] are also compared. (Fig. 8). The GRUMFOIL code consists of a full potential equation flow solver integrated with a viscous boundary-layer model. GRUMFOIL may be entered by specifying either $\bar{\alpha}$ or C_l. The corrected values of Mach number and C_l were used as the input data for the computed results that are compared with the corrected experimental values of C_p shown in Fig. 8. Below each figure are listed M, $\bar{\alpha}$, and C_l values for the tunnel test conditions, corrected values, and values resulting from the GRUMFOIL calculations.

The comparisons between experiment (symbols) and calculations (solid lines) in Fig. 8 are very good. The shock moves aft by approximately 8–10% of chord for a given value of $\bar{\alpha}_t$ when the Reynolds number is increased from 6 to 30×10^6. The GRUMFOIL code underpredicts the position of the shock at both Reynolds numbers by approximately 2–3% of chord even though C_l is matched.

Lift coefficients for several cases are shown in Fig. 9, plotted against corrected angle of attack and against angle of attack as computed by GRUMFOIL for input values of Mach number and C_l for Reynolds numbers of 6 and 30×10^6. The angles calculated from GRUMFOIL are consistently larger than those determined from the correction procedure of Ref. 7. This trend is similar to the one shown in Ref. 9. Irrespective of the angle-of-attack corrections, an increase in C_l of approximately 0.1 is shown as Reynolds number is increased from 6 to 30×10^6. This increase results from the rearward movement of the shock shown in Fig. 8.

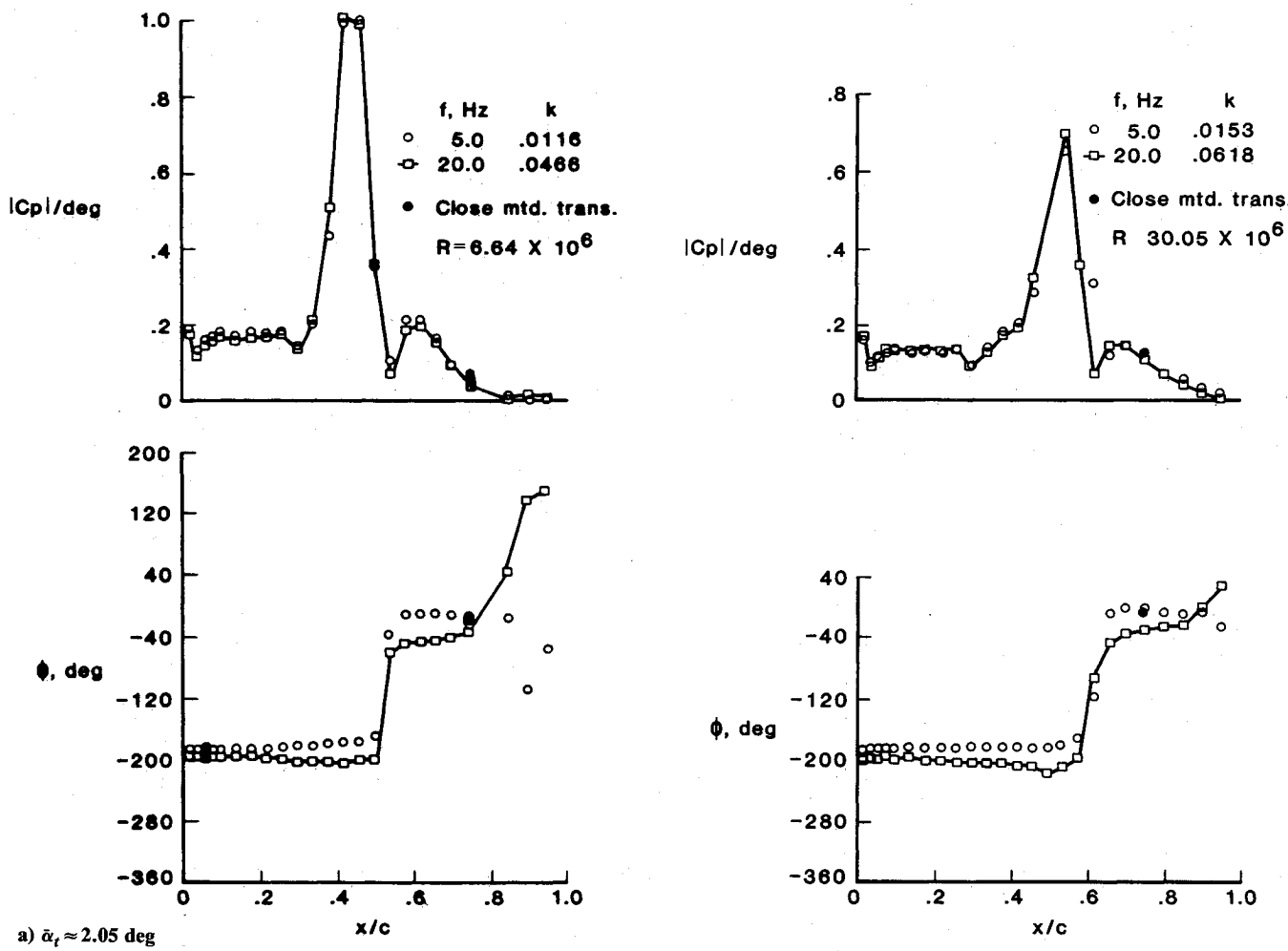

a) $\bar{\alpha}_t \approx 2.05$ deg

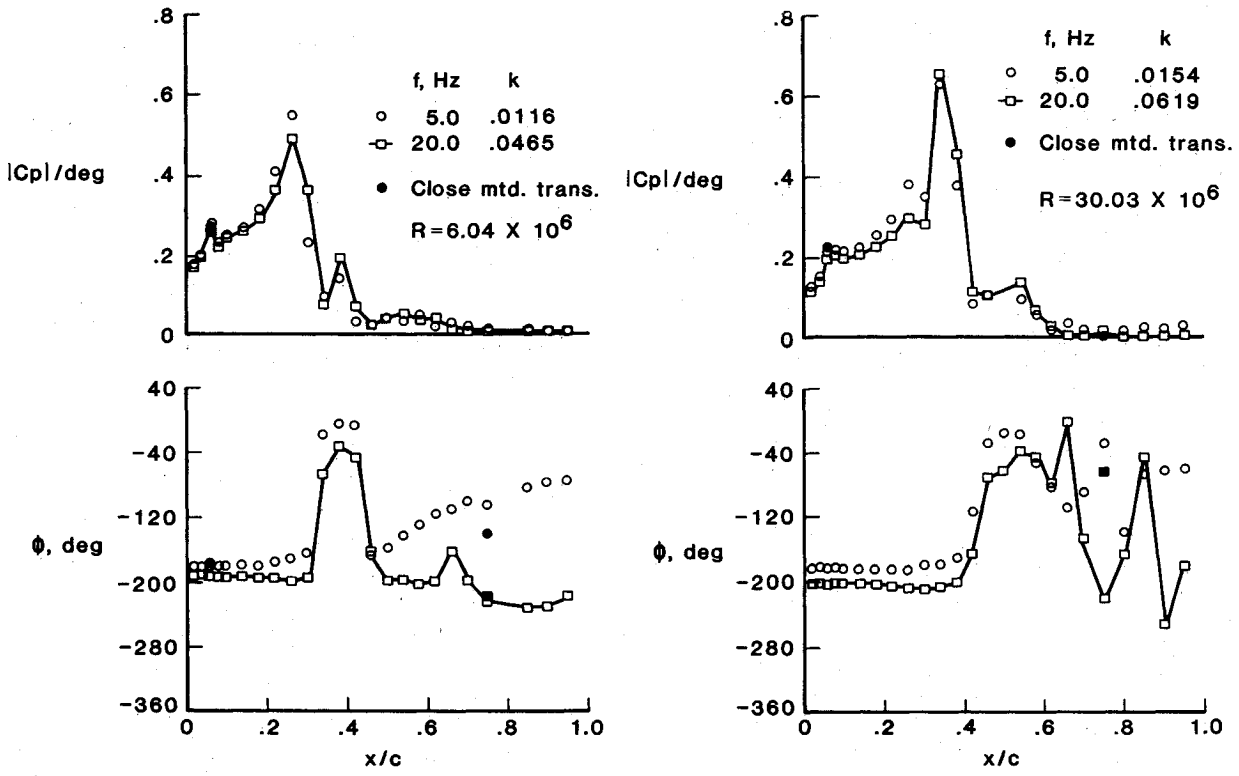

b) $\bar{\alpha}_t \approx 1.04$ deg

Fig. 10 Unsteady pressure test results on the upper surface at a tunnel Mach number of 0.72 and at $\alpha = \pm 0.25$ deg.

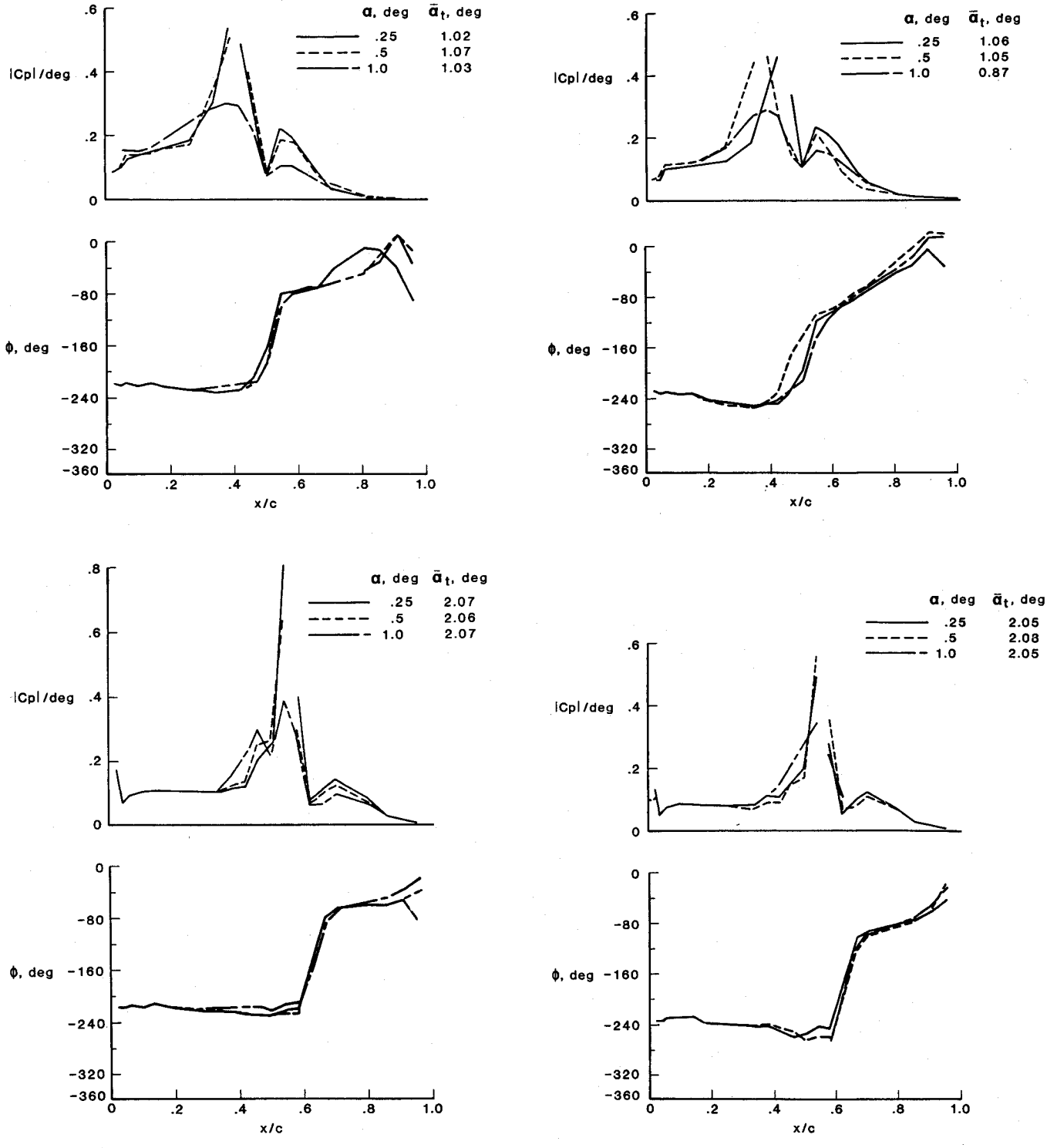

a) $f = 40$ Hz b) $f = 60$ Hz

Fig. 11 Variation of measured $|C_p|$/deg and ϕ with pitch amplitude on the upper surface at $M = 0.72$ and $R = 30 \times 10^6$.

Unsteady Pressures

The effects of Reynolds number and frequency of oscillation on the unsteady pressure distribution are shown in Fig. 10. Results are given in terms of the modulus of the unsteady pressure coefficient normalized by α and the phase angle between the unsteady pressure and the oscillating wing position. Results are shown for $\bar{\alpha}_t = 1$ and 2 deg at Reynolds numbers of 6 and 30×10^6. Two oscillation frequencies, 5 and 20 Hz, are presented for a pitch amplitude of ± 0.25 deg. The upper-surface pressure distributions are shown in Fig. 10.

The shock wave, identified by the peak in the unsteady pressures, moves aft about 8–10% chord as the Reynolds number is increased from 6×10^6 to 30×10^6 at the same test angle of attack. The unsteady pressures, at both Reynolds numbers, are significantly greater ahead of the shock at $\bar{\alpha}_t = 1$ deg than at 2 deg. There is no significant difference in the magnitude of the unsteady pressures due to a change in frequency from 5 to 20 Hz.

For the test conditions shown, the pressures ahead of the shock are approximately 180 deg out of phase with the wing oscillation. Immediately after the shock wave, the pressure phase angle abruptly changes from -180 deg to approxi-

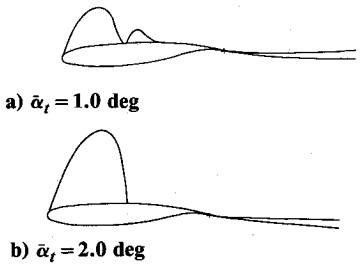

Fig. 12 Sonic regions at $M = 0.72$ calculated by GRUMFOIL code.

mately 0 deg to be in phase with the wing pitching motion. Aft of the shock wave, the phase angle remains at 0 deg at $\bar{\alpha}_t = 2$ deg, but is more dependent on frequency at the lower mean angle of attack ($\bar{\alpha}_t = 1$ deg), tending to go back to -180 deg at 20 Hz and to go to 0 deg at 5 Hz.

The lower-surface pressure magnitude (not shown) is low and decreases from leading to trailing edge. The phase angle is close to zero except at the region of the lower-surface inflection.

The effect of varying the amplitude of the pitch oscillation at $M = 0.72$ is shown in Fig. 11. Unsteady pressure distributions are shown for $R = 30 \times 10^6$ for two mean angles, $\bar{\alpha}_t = 1$ and 2 deg, for the two frequencies, $f = 40$ and 60 Hz. Data for pitch amplitudes of ± 0.25, ± 0.5, and ± 1.0 deg are shown. In most cases, in Figs. 11 and 13, the data points are not connected in the neighborhood of the shock-generated magnitude peak because the peak pressure is not defined by a finite number of pressure orifices. The upper-surface pressure distribution (Fig. 11) shows a reduction and broadening of the shock-generated magnitude peak as α is increased from ± 0.25 to ± 1.0 deg at both frequencies and mean angles. Note the substantial change in mean shock position due to pitch amplitude at $f = 60$ Hz and $\bar{\alpha}_t = 1$ deg.

A secondary peak in the magnitude of the oscillating pressure is evident immediately behind the shock at $\bar{\alpha}_t = 2$ and 1 deg, which could be attributed to flow separation and reattachment as discussed in Ref. 10. However, an inviscid calculation using the XTRAN2L[11,12] computer code predicts this secondary response, albeit not precisely at the same chord location. Calculations with GRUMFOIL (shown in Fig. 12) illustrate that a more probable reason for the secondary response derives from the supersonic regions above the airfoil. At $\bar{\alpha}_t = 1$ deg, there is a secondary supersonic region behind the shock that is engulfed by the primary supersonic region when the angle of attack is increased to $\bar{\alpha}_t = 2$ deg. Tijdeman[13] and others have noted that the flow in the supersonic region prior to the formation of a shock is characterized by a substantial increase in unsteady pressure.

The upper-surface phase angle ϕ shows changes in the neighborhood of the shock and over the aft portion of the airfoil with pitch amplitude (Fig. 11). The lower-surface pressure magnitude and phase ϕ (not shown) are relatively independent of pitch amplitude, except in the neighborhood of the inflection or cusp region of the airfoil. The magnitude is low and decreases from leading to trailing edge.

The effect of varying the oscillation frequency at $M = 0.72$ is shown in Fig. 13. Unsteady pressure distributions are shown for $R = 30 \times 10^6$ for mean angles $\bar{\alpha}_t = 1$ and 2 deg and for pitch amplitudes of ± 0.25 and ± 0.5 deg. Data for frequencies of 5, 15, 40, and 60 Hz are presented. In general, the excursion of the shock on the upper surface (Fig. 13) is reduced at 60 Hz and again the second peak is greater at $\bar{\alpha}_t = 1$ deg than at $\bar{\alpha}_t = 2$ deg and is not a strong function of frequency. As expected, the phase angle is a function of frequency showing characteristics similar to Fig. 10, going to approximately 0 deg behind the shock. The lower-surface pressures decrease from a maximum at the leading edge to a minimum at the trailing edge and show some dependence on frequency.

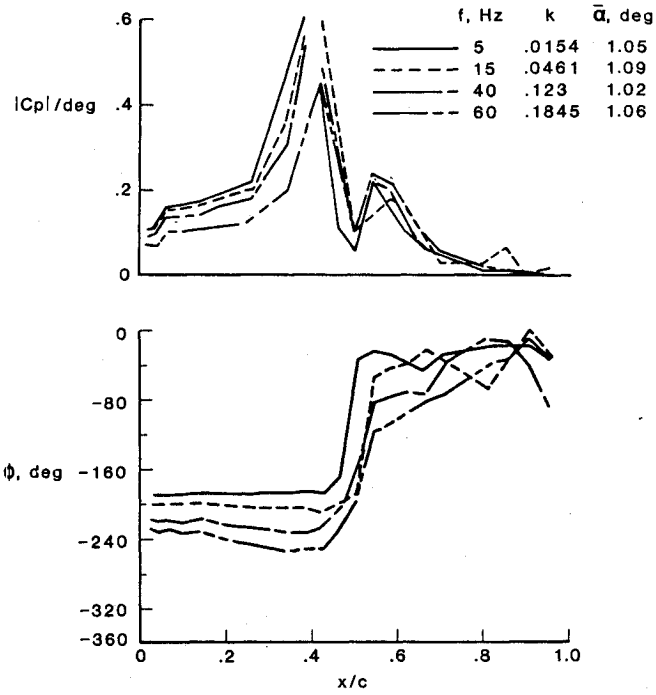

a) $\alpha = \pm 0.25$ deg

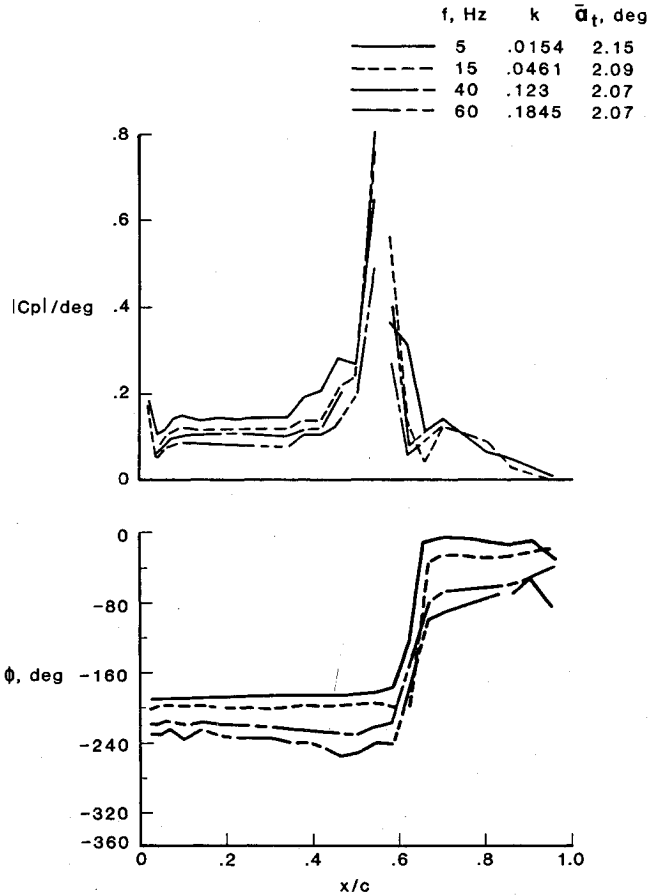

b) $\alpha = \pm 0.5$ deg

Fig. 13 Variation of measured $|C_p|$/deg and ϕ with frequency on the upper surface at $M = 0.72$ and $R = 30 \times 10^6$.

Boundary-Layer State

The unsteady pressure transducers used in this test also recorded measurements of interest regarding the state of the boundary layer. The time histories of the pressures at five transducer locations taken when the airfoil was locked at fixed

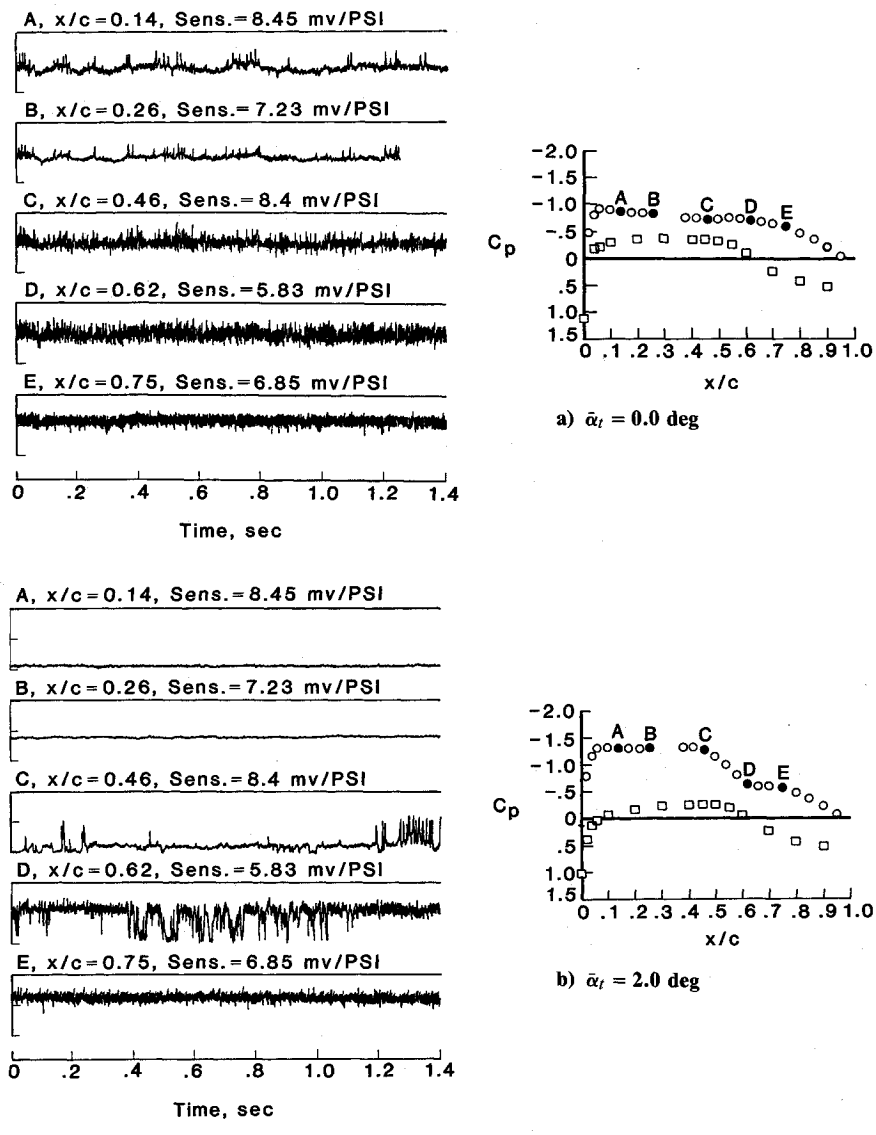

Fig. 14 Time histories at five chord stations for $\alpha = \pm 0.0$ deg, $M = 0.72$, and $R = 35 \times 10^6$ for two steady angles of attack.

angle of attack are shown in Fig. 14. The data shown in this figure are all at a gain of 10 but the transducer sensitivity, given with each trace, has not been applied to put the time histories in engineering units. The time histories taken at two fixed angles of attack ($\bar{\alpha}_t = 0$ and 2 deg) at $R = 35 \times 10^6$ are shown in Figs. 14a and 14b, respectively. The steady pressure distributions are shown at the right of each figure. The solid points on the pressure distribution mark the location ($x/c = 0.14$, 0.28, 0.46, 0.62, and 0.75) of the five transducers. In Fig. 14a ($\bar{\alpha}_t = 0$ deg), the time histories have the characteristics of a turbulent boundary layer. In Fig. 14b ($\bar{\alpha}_t = 2$ deg), the pressure is quiescent at $x/c = 0.14$ and 0.28 in comparison with the transducer responses at $\bar{\alpha}_t = 0$ deg. At an $x/c = 0.46$, the effect of shock movement is observed. At an $x/c = 0.62$, the shock movement is still observed and turbulence is apparent. At $x/c = 0.75$, the signal is comparable to that at $\bar{\alpha}_t = 0$ deg. The most obvious difference between the conditions at the two angles of attack is the presence of a shock and the slightly more favorable pressure gradient at $\bar{\alpha}_t = 2$ deg. The time histories indicate that laminar flow was present at $\bar{\alpha}_t = 2$ deg and that transition to turbulence was between $x/c = 0.28$ and 0.46, corresponding to transition Reynolds numbers between 9.8 and 16.1×10^6. The possibility exists that long runs of laminar flow existed intermittently during the tests.

Conclusions

Steady and unsteady pressures on a 14% thick supercritical airfoil at transonic Mach numbers have been measured at Reynolds numbers from 6 to 35×10^6. Instrumentation techniques were developed to measure unsteady pressures in a cryogenic tunnel at flight Reynolds numbers. Experimental steady data, corrected for wall effects, show very good agreement with calculations from a full potential computer code with an interacted boundary layer. The steady and unsteady pressure both show a shock position that is dependent on Reynolds number. For a supercritical pressure distribution at a chord Reynolds number of 35×10^6, laminar boundary-layer flow was observed over a significant percentage of the airfoil chord.

Acknowledgment

The authors wish to acknowledge the assistance of Clyde Gumbert of the Theoretical Aeodynamics Branch, NASA Langley Research Center, in the GRUMFOIL calculations.

References

[1]Ray, E. J., Ladson, C. L., Adcock, J. B., Lawing, P. L., and Hall, R. M., "Review of Design and Operational Characteristics of the 0.3-m Transonic Cryogenic Tunnel," NASA TM 80123, Sept. 1979.

[2]Ray, E. J., "A Review of Reynolds Number Studies Conducted in the Langley 0.3-m Transonic Cryogenic Tunnel," AIAA Paper 82-0941, June 1982.

[3]Harris, C. D., "Aerodynamic Characteristics of a 14-Percent Thick NASA Supercritical Airfoil Designed for a Normal-Force Coefficient of 0.7" NASA TM X-72712, July 1975.

[4]Jenkins, R. V., Hill, A. S., and Ray, E. J., "Aerodynamic Performance and Pressure Distributions for a NASA SC(2)-0714 Airfoil Tested in the Langley 0.3-Meter Transonic Cryogenic Tunnel," NASA TM 4044, July 1988.

[5]Sewall, W. G., "The Effects of Sidewall Boundary Layer in Two-Dimensional Subsonic and Transonic Wind Tunnels," *AIAA Journal,* Vol. 20, Sept. 1982, pp. 1253–1256.

[6]Jenkins, R. V. and Adcock, J. B., "Tables for Correcting Airfoil Data Obtained in the Langley 0.3-Meter Transonic Cryogenic Tunnel for Sidewall Boundary Layer Effects," NASA TM 87723, June 1986.

[7]Barnwell, R. W., "Design and Performance Evaluation of Slotted Walls for Two-Dimensional Wind Tunnels," NASA TM 78648, Feb. 1978.

[8]Mead, H. R. and Melnik, R. E., "GRUMFOIL: A Computer Code for the Viscous Transonic Flow Over Airfoils," NASA CR 3806, Oct. 1985.

[9]Gumbert, C. R. and Newman, P. A., "Validation of a Wall Interference Assessment/Correction Procedure for Airfoil Tests in the 0.3-m Transonic Cryogenic Tunnel," AIAA Paper 84-2151, Aug. 1984.

[10]Mundell, A. R. G. and Mabey, D. G., "Pressure Fluctuations Caused by Transonic Shock/Boundary-Layer Interaction" *Aeronautical Journal,* Vol. 90, Aug./Sept. 1986, pp. 274–282.

[11]Whitlow, W., Jr., "XTRAN2L: A Program for Solving the General Frequency Unsteady Transonic Small Disturbance Equation," NASA TM 85721, Nov. 1983.

[12]Seidel, D. A. and Batina, J. T., "User's Manual for XTRAN2L (Version 1.2): A Program for Solving the General-Frequency Unsteady Transonic Small-Disturbance Equation," NASA TM 87737, July 1986.

[13]Tijdeman, H., "Investigation of the Transonic Flow Around Oscillating Airfoils," NLR TR 77090 U, Oct. 1977.